Cellulose and chitosan derivatives for enhanced sorption of erbium(III)

Mahmoud O. Abd El-Magied, Ahmed A. Galhoum, Asem A. Atia, Ahmad A. Tolba, Mai S. Maize, Thierry Vincent, Eric Guibal

Cellulose and chitosan derivatives for enhanced sorption of erbium(III)

Mahmoud O. Abd El-Magied[a], Ahmed A. Galhoum[a,b], Asem A. Atia[c], Ahmad A. Tolba[a], Mai S. Maize[c], Thierry Vincent[b], Eric Guibal[b,*]

[a] *Nuclear Materials Authority, P.O. Box 530, El-Maadi, Cairo, Egypt*
[b] *Ecole des mines d'Alès, Centre des Matériaux des Mines d'Alès, 6 avenue de Clavières, F-30319 Alès cedex, France*
[c] *Chemistry Department, Faculty of Science, Minoufia University, Shabin El-Kom, Menoufia, Egypt*

ABSTRACT

Cellulose (Cell) was chemically modified by grafting thiourea (Thio-Cell) and glutaraldehyde cross-linked chitosan (GLA-Chit) was functionalized by poly(aminocarboxymethylation) (PCM-Chit); material was also pre-pared as a composite material that incorporates a magnetic core (Magn PCM-Chit). The sorption properties of these materials have been compared to non-modified cellulose and GLA-Chit for Er(III) uptake. Sorption in-creases with progressive deprotonation of reactive groups, such as R—OH, R—SH, amine and carboxylic acid groups. The chemical modification significantly increases sorption performance and more specifically the poly (aminocarboxymethylation): sorption capacities increase up to 117–145 mg Er(III) g^{-1}. Sorption capacities also increase with temperature: the sorption is endothermic and spontaneous. The spontaneity of the reaction sig-nificantly increases with chemical modification of chitosan-based sorbent. The entropy of the system is negative for GLA-Chit, Cell and Thio-Cell and positive for PCM-Chit materials. Acidic solutions of thiourea efficiently desorb Er(III) and allows the recycling of the sorbents for a minimum of 5 sorption/desorption cycles. FT-IR spectrometry, XRD, TGA, elemental analyses and SEM observations have been used for characterizing the ma-terials. The magnetic properties of Magn PCM-Chit were also characterized by VSM.

Keywords:
Cellulose
Chitosan
Chemical modification
Poly(aminocarboxymethylation)
Thiourea derivative of cellulose
Magnetic sorbent
Erbium
Uptake kinetics
Sorption isotherms
Desorption
Thermodynamics

GRAPHICAL ABSTRACT

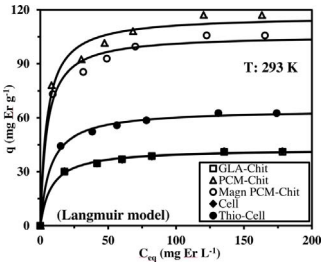

1. Introduction

The increasing demand for rare earth elements (REEs) is driven by the development of high-tech products including photonics and electronic devices, high-performance ceramics and glasses, alloys and magnets. For some of them, the demand exceeds the annual production making these materials strategic and critical [1]. In addition, the production is concentrated in a limited number of countries; China having a quasi-monopoly for some of these REEs. Recently, numerous mining projects have been launched for producing REEs and for winning industrial supply independency. Incentive politics have also been initiated for promoting the recovery of REEs from secondary resources

* Corresponding author.
E-mail address: eric.guibal@mines-ales.fr (E. Guibal).

[2], including low-grade ores, mining residues, waste materials; this has motivated an increasing number of studies in the field of hydrometallurgy [3–8].

Leaching of electronic wastes or minerals produces, in most cases, acidic solutions containing traces or low-concentrations of REEs [9]. The treatment of these leachates may involve processes such as solvent extraction [7,10], precipitation [11] for high-concentration effluents and sorption processes for more diluted effluents. Mineral sorbents [12,13], ion-exchange or chelating resins can be used [14–19]; however, in the case of very dilute effluents, biosorbents may be an interesting alternative [20,21]. These materials produced from renewable resources such as agriculture or marine feedstock bear the same functional groups as those found on synthetic resin [22,23]. Their availability and their low cost contribute to make them competitive; in addition, they may be readily modified chemically by grafting new functional groups [24], or physically by conditioning under the form of beads, magnetic particles (for example) [25,26].

Chitosan, an aminopolysaccharide produced from crustacean shells, and cellulose are abundant polysaccharides that can be used for metal binding [27,28]. However, these materials have relatively low sorption capacities for REEs and it is generally necessary grafting specific functional groups on their polymer backbone [29–34] or incorporating other ion-exchanger [35] for reaching significant sorption capacities.

The affinity of metal ions for specific functional groups is controlled by the so-called HSAB theory, Hard and Soft Acid Base theory, also called Pearson rules [14,36,37]. In addition, steric effects may influence metal binding; this may influence more specifically sorption selectivity when various metal ions are present in the solution. Ionic radii can then be considered for correlating sorption efficiencies and capacities with steric parameters. Chung et al. [38] reported the modification of silica foams by functionalization with multi-amine groups and they observe that the sorption does not increase with the density of amine groups. They explain this unexpected result by two possible steric effects: (a) pore blockage, and (b) a conformational change of available amine groups. Yang and Alexandratos [14] also commented the influence of additional criteria such as the hydration of the REEs, and the coordination properties of the counterion on RE affinity testing several ligands. This study investigates the sorption of Er(III) using cellulose and chitosan derivatives bearing different functional groups: sulfur groups on cellulose (Thio-Cell), carboxymethyl and amino groups on chitosan (after functionalization, PCM-Chit). The sorption properties of these derivatives have been compared to those of non-modified cellu-lose (-OH reactive groups, Cell), and simply glutaraldehyde crosslinked chitosan (-OH and amine reactive groups, GLA-Chit). In addition a composite material associating magnetic core with functionalized chitosan coating has also been tested for Er(III) sorption (Magn PCM-Chit). Nano- or micro-based magnetic particles can be “decorated” with chitosan and derivatives for metal recovery with the double objective: (a) high sorption capacities derived from chemically modified polymer and (b) fast kinetics, due to the thin layer of polymer deposited on the magnetic core and limited resistance to intraparticle diffusion. Small particles present the advantage of reducing the potential impact of resistance to diffusion and improving mass transfer, at the expense of making the management of particles relatively difficult through pressure drop when applied in columns, hydrodynamic blockage or difficult solid/liquid separation in batch reactor. Incorporating a magnetic core in micro-particles allows improving the recovery of metal-loaded particles at the end of the process [33,39]. Structured materials, such as beads, rods (for example) having appropriate spherical shaping for enhanced hydrodynamic properties and high porous properties, for negligible resistance to intraparticle diffusion, are well designed for application in fixed-bed systems or chromatography applications. On the other hand, in batch systems, the resistance to intraparticle diffu-sion may control uptake kinetics and decreasing the size of sorbent particles contributes to improving mass transfer. Incorporating a mag-netic core in the micro- or nano-particles facilitates the solid/liquid separation at the end of the process. Magnetic particles are also facilitating the safe recovery of spent sorbents at the end of the process when applied in hazardous environments (for example in nuclear industry).

These materials have been systematically tested for Er(III) sorption using similar procedures. Though erbium is less critical than some other rare earth metals it is representative to the class of heavy REEs and poorly documented in the literature. It appeared interesting evaluating the sorption properties of Er(III) as an example of HREEs. The materials are first characterized using elemental analysis, FTIR spectrometry, XRD analysis, vibrating sample magnetometry (VSM, for magnetic material), TGA analysis. In a second step the sorption properties are carried out through the study of: (a) pH effect, (b) uptake kinetics, (c) sorption isotherms including thermodynamic parameters and (d) metal desorption/sorbent recycling.

2. Materials and methods

2.1. Materials

Chitosan (90.7% deacetylation), glutaraldehyde (50%, w/w), epichlorohydrin (> 98%), thiourea, phosphorus oxychloride ($POCl_3$) and monochloroacetic acid were supplied by Sigma-Aldrich (Saint Quentin Fallavier, France). Microcrystalline cellulose was obtained from Merck (Darmstadt, Germany). Ethanol, *N*-*N*-dimethylformamide (DMF) and 1,4-dioxane (99.9%) were purchased from Fluka Chemicals (Buchs, Switzerland). Other chemical reagents were supplied by VWR BDH Prolabo Chemicals (Fontenay-sous-Bois, France). Erbium was purchased from Alfa-Aesar (Heysham, UK): $ErCl_3{\cdot}xH_2O$ salt was burned off at 900 °C for 3 h before being completely dissolved in concentrated HCl under heating; the solution was diluted with Milli-Q water. The concentration of stock solution was 1000 mg Er L^{-1}.

2.2. Synthesis of sorbents

Chitosan being soluble in acidic solution (at the remarkable exception of sulfuric acid) the biopolymer was first crosslinked with glutaraldehyde. Chitosan (4 g) was dissolved in 200 mL of acetic acid (5% w/w) under agitation overnight. The polymer solution was distributed dropwise through a thin nozzle (0.8 mm internal diameter) into a neutralization bath (2 M NaOH solution) to prepare chitosan beads. After abundant rinsing the beads were dropped into a glutaraldehyde solution (2.5% w/w) for 24 h at room temperature: the molar ratio between amine groups (on the biopolymer) and aldehyde groups (on the crosslinking agent) was set to 1:1. The GLA-Chit beads were filtrated, washed with ethanol and water before being dried and finally crushed to final size below 250 µm.

Cellulose (Cell) and GLA-Chit were functionalized through a two-step procedure: first the biopolymers were chlorinated, before being chemically grafted (Figs. 1 and 2). The chlorination took place in DMF: the polymers (4 g) were mixed with the solvent for 1 h at 25 °C before adding 9 mL of $POCl_3$. The reaction was continued for 1 h at 75–80 °C for chitosan-based sorbents and for 1 h at 75–80 °C for cellulose-based sorbent. The chlorinated materials were successively washed with ice-water, DMF and demineralized water (at room temperature) [40–42].

Thio-Cell was obtained by reaction of the intermediary product (3 g) with thiourea (5.7 g) and Na_2CO_3 (0.33 g) in 60 mL of Milli-Q water, under reflux for 24 h [42]. After repeated rinsing to remove unreacted reagents the material was filtered and freeze-dried for 24 h.

The PCM-Chit was prepared by a first reaction of chlorinated GLA-Chit with 16 mL of tetraethylenepentamine (TEPA, 16 mL) in 200 mL of ethanol/water solution (1:1, v/v) for 18 h at 80–85 °C, under reflux. After being abundantly rinsed (with water and ethanol) and dried, the intermediary product was reacted with 28 g of monochloroacetic acid (for 4 g of initial amount of chitosan) in dioxane (100 mL) under reflux for 18 h (after adjusting the pH to 9–9.5 using 1 M NaOH solution). The

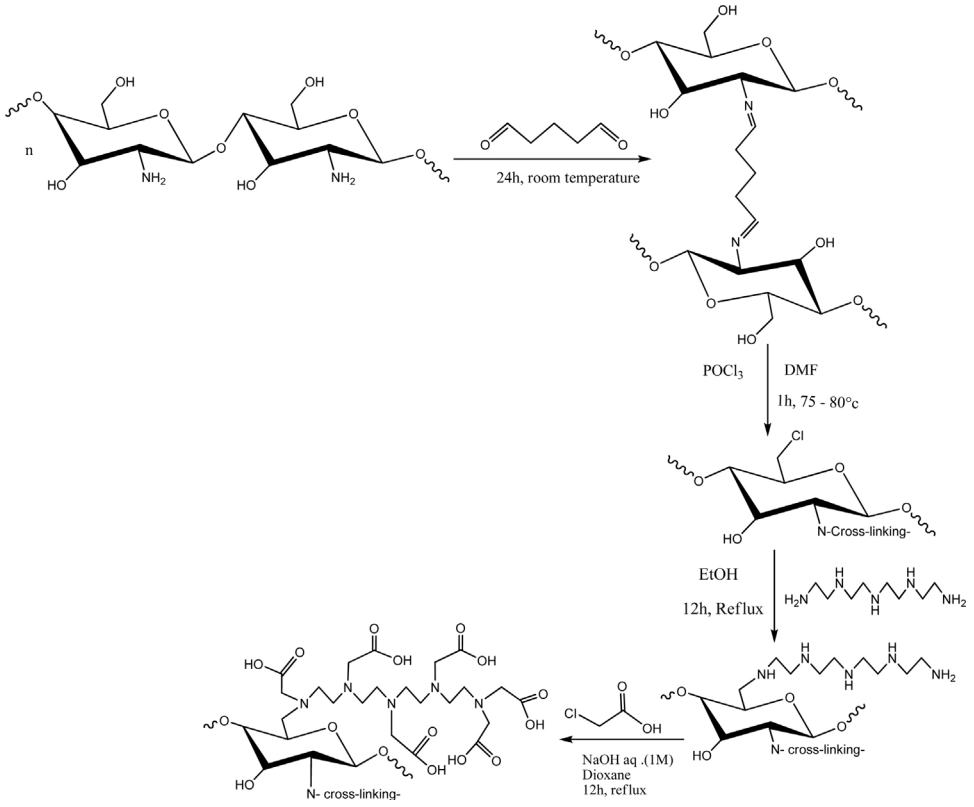

Fig. 1. Scheme for the synthesis of PCM-Chit.

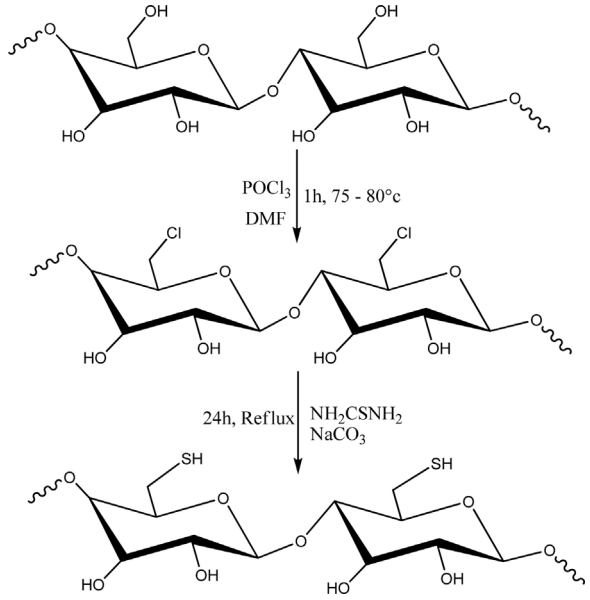

Fig. 2. Scheme for the synthesis of Thio-Cell.

final product was filtrated and washed with ethanol and Milli-Q water. Finally, the carboxylic groups on the sorbent were converted to carboxylate by mixing the sorbent with a 0.2 M NaOH solution for 30 min. After rinsing, the sorbent was freeze-dried for 24 h.

The synthesis of Magn PCM-Chit followed a modified amino-carboxymethylation procedure. The first difference consisted of the incorporation of a magnetic core produced in situ in the chitosan hydrogel [33,43]. Chitosan (4 g) was dissolved in 200 mL of acetic acid (5% w/w) before adding $FeSO_4$ and $FeCl_3$ salts (respecting a Fe(II)/Fe (III) molar ratio of 1:2; i.e., 1.66 g of $FeSO_4{\cdot}7H_2O$ and 2.17 g of $FeCl_3$). The mixture was pumped through a thin nozzle into a 1 M NaOH solution (final pH close to 10). The suspension was then heated at 90 °C under reflux and stirring for 1 h. The beads were then washed with demineralized water and crosslinked with glutaraldehyde (2.5% w/w solution and stoichiometric ratio 1:1 between aldehyde groups and amino groups) for 24 h at room temperature. Crosslinked magnetic chitosan particles were suspended into 200 mL of ethanol/water (1:1, v/v) solution in the presence of 15 mL of epichlorohydrin under agitation and heating under reflux for 4 h. After careful rinsing, with ethanol and Milli-Q water, the material was suspended into 200 mL of ethanol/water mixture in the presence of 16 mL of tetraethylenepentamine under agitation and reflux for 8 h. The solid was filtrated, rinsed with ethanol and Milli-Q water before adding monochloroacetic acid (28 g) in dioxane at pH 9–9.5, controlled with 1 M NaOH solution, under reflux. After rinsing the sorbent was conditioned under the carboxylate form by immersion in a 0.2 M NaOH solution for 30 min. The washed material was finally freeze-dried and crushed to a size below 250 µm.

2.3. Characterization of sorbents

The chemical composition of the sorbents was determined using an automatic analyzer (CHNS Vario EL III Elementar analyzer, Elementar, Langenselbold, Germany). A Jasco FT-IR-6600 spectrometer (Jasco, Easton, MD, USA) was used for the FT-IR analysis of the materials. The pH_{ZPC} of the materials was determined by the pH-drift method: the sorbents were equilibrated under agitation for 48 h with a series of 0.01 or 0.1 M NaCl solutions with different initial pH values (pH_i); the equilibrium pH (pH_{eq}) was recorded and the pH_{ZPC} is the pH value corresponding to $pH_i = pH_{eq}$ [44]. X-ray diffraction-analyses were performed at room temperature on an X-ray diffractometer (SmartLab Rigaku, Tokyo, Japan; Cu K_α radiation and angle range 2θ: 20–80°). Thermal degradation properties were obtained using a TG/DTA analyzer (Seiko 633N EXSTAR TG/DTA, Seiko Instruments, Chiba, Japan; N_2/O_2 atmosphere, temperature range: 20–900 °C with a temperature ramp of 20 °C min^{-1}).

2.4. Metal sorption and desorption

Sorption experiments were performed, in batch mode, by contact under agitation (200 rpm) of a mass of sorbent (m, g) with given volume (V, L) of solution at fixed initial metal concentration (C_0, mg Er L^{-1}) and fixed pH, controlled with 0.05–1 M solutions of either HCl or NaOH. The pH was not controlled but was systematically monitored at the end of the sorption process. Temperature was set at 27 ± 1 °C except for the study of thermodynamic parameters. At given contact times samples were collected, filtrated and analyzed for residual concentration (C(t) or C_{eq}, mg Er L^{-1}) using an ICP-AES (inductively coupled plasma atomic emission spectrometer, Activa M, Horiba France, Longjumeau, France). For sorption isotherms the contact time was set at 4 h; this contact time is sufficient for reaching the equilibrium. The sorption capacity (q, mg Er g^{-1}) was calculated by the mass balance: $q = (C_0 - C_{eq}) \times V/m$. The experimental conditions were varied for evaluating specific sorption properties: the complete experimental conditions are briefly reported in the caption of the relevant Figures (or Tables).

Desorption tests were performed by contact, under agitation for 1 h at 27 °C, of Er-loaded sorbents with a 0.5 M solution of thiourea, acidified with sulfuric acid at pH 2. After filtration, the amount of metal eluted was compared to the amount of metal sorbed at each stage for calculating the desorption efficiency; the sorbed amounts at each stage were compared to the sorption at the first cycle. After each desorption step the sorbent were conditioned under the form of carboxylate groups, when relevant (for PCM-Chit type sorbents) by immersion of the sorbent into 0.2 M NaOH solutions for 30 min and water rinsing.

2.5. Models

Uptake kinetics may be controlled by several mechanisms such as resistances to film diffusion and to intraparticle diffusion, proper reaction rate, which may be described by the pseudo-first order rate equation, PFORE or the pseudo-second order rate equation, PSORE [45–47]. The sorption isotherms represent the distribution of metal species between liquid and solid phases at equilibrium [47–50]. These models are detailed in Additional Material Section.

3. Results and discussion

3.1. Synthesis and characterization of sorbents

3.1.1. Elemental analysis

The elemental analysis of the materials at different stages of the synthesis procedure (Table 1) confirms the suggested mechanisms of chemical modification of chitosan and cellulose (Figs. 1 and 2). The chlorination of the biopolymer reduces the C and N mass fractions in the materials. After polyamination the mass fraction of nitrogen strongly increases: the chlorinated GLA-Chit contains 3.23 mmol N g^{-1}, while after polyamination the molar content is 7.05 mmol N g^{-1} (with simultaneous increase of C mass fraction to a level comparable to the C content analyzed in GLA-Chit material). After carboxylation the fraction of nitrogen is significantly decreased: the relative increase of the molar mass may explain this decrease; the N content decreases to 4.83 mmol N g^{-1} in the final product.

In the case of Thio-Cell, the grafting of thiourea is confirmed by the presence of S element: S molar content approaches 0.59 mmol S g^{-1}.

Table 1
Elemental analysis of sorbents (and intermediary materials).

Sorbent	C(%)	H(%)	N(%)	S(%)
Chitosan	40.00	6.88	7.47	–
GLA-Chitosan	44.57	6.46	5.33	–
Chlorinated GLA-Chitosan	37.98	5.35	4.53	–
Polyaminated-Chitosan	44.02	6.37	9.88	–
PCM-Chitosan	44.21	5.97	6.77	–
Magn PCM-Chitosan	40.27	5.19	7.14	–
Cellulose	42.67	6.41	–	–
Chlorinated Cellulose	33.68	4.66	–	–
Thio-Cellulose	34.53	5.19	–	1.89

3.1.2. Sorbent morphology

The Fig. 3 shows the morphology of sorbent particles. The fibrillary structure of cellulose material is significantly changed after chemical modification of the biopolymer: layered structures are formed with small aggregates. In the case of chitosan-based materials, the smoothed surface of GLA-Chit is turned to very irregular aggregates for PCM-Chit while for Magn PCM-Chit massive blocks were formed with well-delimited linear edges. The structure is more compact than with PCM. This could be attributed to the magnetite core that maintains the structure of the material during the drying step, contrary to chitosan gel whose structure collapses when dried. The size of sorbent particles was 63–125 µm for synthesized materials after grinding and sieving while the size of Cell particles was the original size of commercial cellulose (commercial data for Avicel Merck cellulose: 80 µm).

3.1.3. FTIR analysis

FT-IR spectroscopy allows identifying the reactive groups on the sorbents (Fig. AM1, see Additional Material Section) and the successive chemical modifications of the biopolymers. The spectrum of cellulose is characterized by the usual bond vibrations [51,52]:

- 3300–3400 cm^{-1}: large band corresponding to ν(OH) stretching in the polysaccharide ring, and −CH−OH, $-CH_2-$OH side chain stretching,
- 2885–2890 cm^{-1}: stretching of methylene groups,
- 1309 cm^{-1} and 1109 cm^{-1}: stretching of primary and secondary −OH groups, respectively,
- 1433 cm^{-1}, assigned to C−O−C stretching or $-CH_2$ bending mode, and 1304 cm^{-1} attributed to −OH bending,
- 889–898 cm^{-1}: β-D-glucose unit: C−O−C stretching.

The chlorination of cellulose is confirmed by the appearance of bands in the range 700–760 cm^{-1}, assigned to $\nu(CH_2-Cl)$ and the relative decrease in the intensities of the bands at 3300–3400 cm^{-1}, 1500 cm^{-1} and 1200 cm^{-1}, which are explained by the substitution of hydroxyl groups at C_6 position [53–55]. The further grafting of thiourea leads to a decrease in the intensity of the bands in the range 760–700 cm^{-1} as a confirmation of the grafting mode. The −SH bands are difficult to identify due to (a) the low amount of sulfur immobilized on the polymer backbone (0.59 mmol g^{-1}), and (b) the poor sensitivity of the relevant signals (at 630–710 cm^{-1} [53], 1059 cm^{-1} [56] and 2550 cm^{-1} [54]).

For chitosan-based materials the main FTIR bands have been reported [51,57,58]:

- 3420–3450 cm^{-1}: superimposition of N−H and O−H stretching,
- 2877 cm^{-1}: stretching C−H,
- 1620–1670 cm^{-1}: C=O stretching in secondary amide I [59] or C−N−H in amide I [51],
- 1550–1570 cm^{-1}: C=O stretching in secondary amide II, [59] or δ(NH), [58],
- 1420–1450 cm^{-1}: amide II groups [57], or C−OH linkage [51],
- 1380 cm^{-1}: C−O groups [57], or CH_2 groups,
- 1159 cm^{-1}, 1075 cm^{-1} and 1025 cm^{-1}: C−O−C groups in polysaccharide ring [51,58],
- 896 cm^{-1}: C−N finger-print.

The crosslinking of chitosan with glutaraldehyde leads to the appearance of −CO−NH groups and the reinforcement of the signals

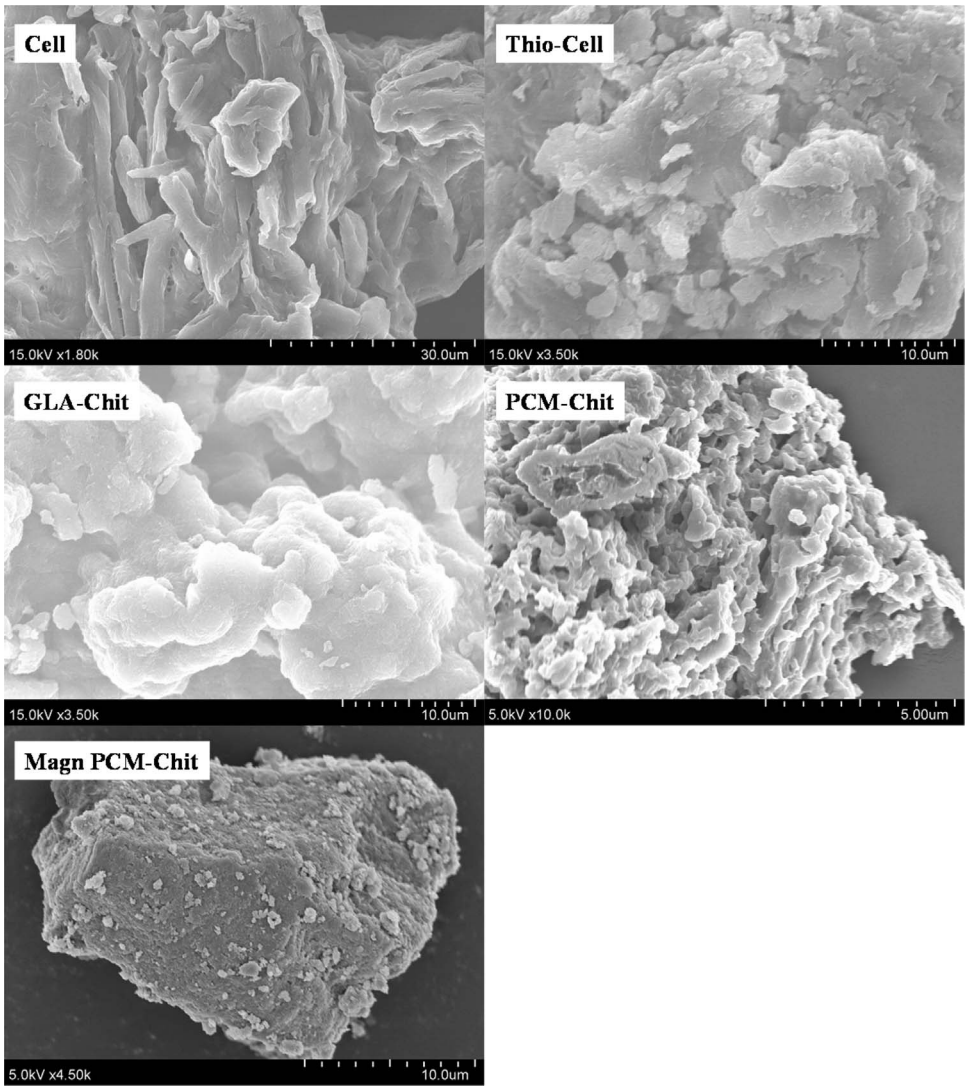

Fig. 3. Morphology of sorbents (SEM micrographs) (Magnification: ×1800–4500).

corresponding to amide groups. After chlorination the typical band at 700–760 cm^{-1}, assigned to $\nu(CH_2—Cl)$, is appearing. After TEPA-grafting, the signal for chlorinated groups is weakened while the intensity of primary and secondary amine groups are increased at 1300–1500 cm^{-1} and 1600 cm^{-1} [55]. In the next step of the process, the carboxymethylation of amine groups leads to a decrease in the intensity of amine groups and the appearance of a signal corresponding to carboxyl groups,at around 1730 cm^{-1} [55].

3.1.4. pH_{zpc}

The pH-drift method was tested for different experimental concentrations (sorbent dosage, concentration of the background salt: 0.01 and 0.1 M NaCl solutions, contact time: 24 and 48 h); an example is given in Fig. 4. The pH_{ZPC} of the different sorbents were obtained. The grafting of thiol groups on cellulose hardly changes the pH of zero charge of the sorbent: 6.21 ± 0.33 and 6.26 ± 0.46 for Cell and Thio-Cell, respectively. While GLA-Chit has a pH_{ZPC} close to the values of cellulose-based materials (i.e., 7.05 ± 0.61), the chemical modification of the aminopolysaccharide strongly affects the value of the pH of zero charge. Indeed, after poly(aminocarboxymethylation) the pH_{ZPC} of the sorbent drops to 4.12 ± 0.26. This can be easily explained by the immobilization of carboxylic acid groups, with pK_a lower than 4. This is another proof that the chemical grafting is efficiently operated on the biopolymer backbone to bring acidic functions. In the case of magnetic-based sorbent the decrease in the pH of zero charge is less marked: the

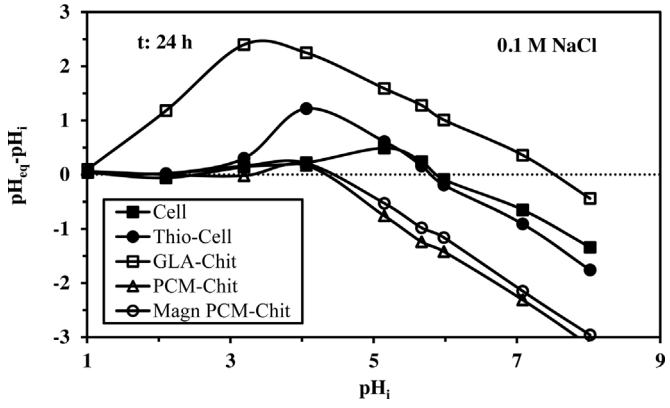

Fig. 4. Determination of pH_{ZPC} for the sorbents by the pH-drift method – determination of the pH corresponding to $pH_i = pH_{eq}$ (Example of test performed with Sorbent dosage: 1 g L^{-1}; Background salt: NaCl (0.1 M); agitation time: 24 h).

pH_{ZPC} tends to 4.44 ± 0.02. These results are consistent with literature data. Glutaraldehyde crosslinking of chitosan hardly changes the pH_{ZPC} of chitosan, in the range 6–7 [60]. Igberase et al. reported that the grafting of ethylenediaminetetraacetic acid on chitosan contributes to decrease the pH_{ZPC} to 4.4 [61]. In the case of cellulose-based sorbent, Silva et al. [62] demonstrated that the grafting of aminoethanethiol did not change the pH_{ZPC} that remains close to 6; the pH_{ZPC} of cellulose

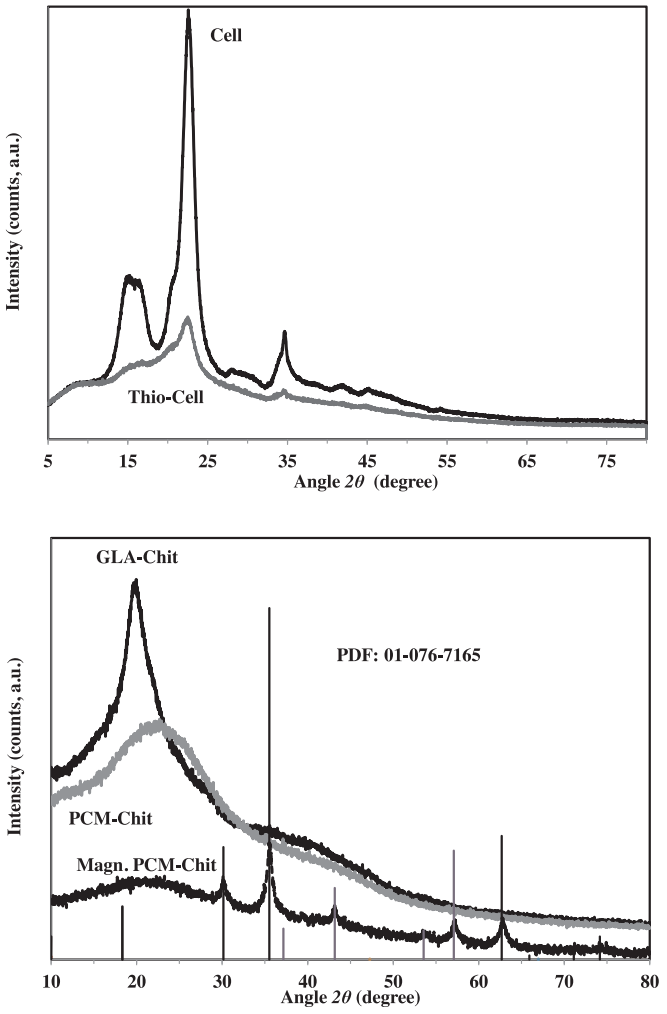

Fig. 5. XRD patterns for GLA-Chit; PCM-Chit, Magn PCM-Chit, Cell and Thio-Cell (the bar-type spectrum represents the XRD referenced pattern of magnetite).

close to 6 is slightly increased to 6.5 after being reacted with epichlorohydrin [63].

3.1.5. XRD analysis

The X-ray diffraction patterns have been compared for the different materials (Fig. 5). Cellulose is characterized by 4 peaks corresponding to 2θ angles: 15.1°, 16.4°, 22.6° ($1\bar{1}0$, 110, 020 lattice planes of cellulose I) [64] and 34.6° (004 lattice plane of cellulose) [65]. After chemical modification, the arrangement of polymer chains is strongly affected: the grafting of chemical groups induces hydrolytic cleavage of glycogenic bonds, release of crystallites, the breakage of hydrogen bonds in the crystalline part of the polymer [66] and the intercalation of molecules that decrease the ordered arrangement of the polymer structure. As a consequence the crystallinity of the modified polymer is strongly decreased: the intensity of the peaks is drastically diminished, the only detectable peak corresponds to the peak at 22.6°. Similar loss in the crystallinity of cellulose was obtained for other chemical derivatives [54,55,66]. In the case of GLA-Chit and derivatives the materials are poorly crystalline. The unique peak is relatively large and is located close to 2θ = 20° ([67]). After chemical modification the crystallinity is drastically reduced: the peak is broadened and shifted toward higher 2θ (i.e., close to 23°). The intercalation of reactive groups in the polymer network and the disruption of hydrogen bonds between the chains can explain this decrease of the crystallinity: the structure is less organized. Similar change in the crystallinity of chitosan was observed in the case of papain incorporation into chitosan beads crosslinked with tripolyphosphate and/or glutaraldehyde [67]. The incorporation of a magnetic core in the sorbent particle, by in situ synthesis, is confirmed by the appearance of typical peaks of magnetite phase at 2θ ≈ 30°, 35°, 43°, 53°, 57° and 62° [68].

3.1.6. Magnetic properties

The magnetic properties of Magn PCM-Chit sorbent have been analyzed by VSM (Fig. AM2, see Additional Material Section). The absence of coercivity and remanence indicates that the material has superparamagnetic properties [69]. The saturation magnetization of the sorbent is relatively low (i.e., 5.4 emu g^{-1}). The magnetization of magnetite particles coated with chitosan derivative is relatively small compared to conventional values of magnetite nanoparticles (usually in the range 50–80 emu g^{-1}) [68]. This may be attributed to the very low amount of magnetite in the composite sorbent (i.e., close to 7.7% w/w, based on weight loss studies). The magnetization of the composite is supposed to be proportional to the fraction of magnetite [70–72,68,69]. However, this is sufficient for achieving the magnetic separation of sorbent particles from solution.

3.1.7. Thermal properties

Thermal degradation of sorbents has been carried out under N_2/O_2 atmosphere; i.e. aerobic thermal degradation. Fig. 6 reports the different TGA profiles. Cellulose material is characterized by a first step that corresponds to the release of absorbed and structural water, after 280 °C a strong weight loss is observed (sharp curve) till 340–350 °C; this corresponds to the thermal degradation of cellulose which is followed by the combustion of the char above 350 °C that finished at the temperature of 670 °C. In the case of Thio-Cell, the degradation profile is more complex; this is due to the decomposition of the functional groups grafted on the cellulose backbone; i.e., chlorination spacer, and more specifically thiourea. Water removal corresponds to 25–185 °C temperature range, while above 190 °C a series of degradation phases (4 steps) are observed: (a) a small weight loss (about 12%) between 190

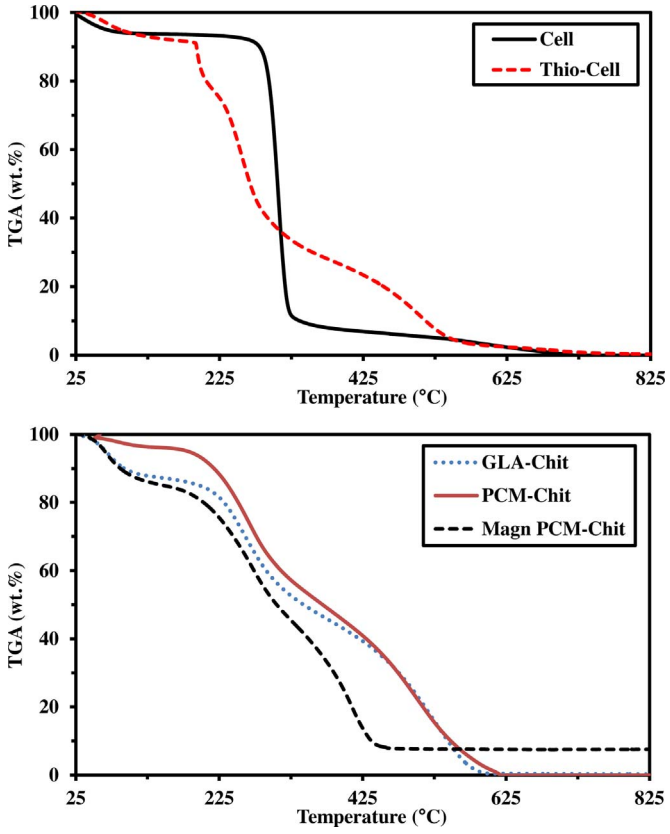

Fig. 6. TGA analysis of sorbents.

and 202 °C, (b) a progressive weight loss between 202 °C and 285 °C (about 48%), (c) a progressive and "slow" degradation that corresponds to the thermal degradation of the char, which represents 25% of the weight, between 285 °C and 545 °C, and (d) a linear degradation curve for the combustion of the remaining material (about 5%) until 700 °C. The first two steps of this process are probably associated to the degradation of the chemical groups and the cellulose backbone, respectively. In the case of chitosan-based sorbents, the water removal occurs between 180 and 205 °C, depending on the sorbent, and the loss represent between 5 and 18%. Above 200 °C the thermal degradation of the chitosan derivatives is characterized by two phases: (a) between 205 °C and 300 °C, the chemical groups (glutaraldehyde for GLA-Chit and poly(carboxymethyl) groups, and probably intermediary TEPA anchoring groups, for PCM-Chit) are progressively decomposed; (b) above 300 °C (till 580–615 °C) the degradation of the chitosan backbone and further combustion of the char. The degradation profiles are similar for GLA-Chit and PCM-Chit; the only significant difference is observed at the beginning of the thermogram: the initial weight loss is lower for chemically grafted sorbent. This is probably associated to a lower absorption of water or weaker water retention in the modified material; above the temperature of 240 °C, the thermodegradation profiles are very close for the precursor and the modified material. In the case of Magn PCM-Chi, the TGA thermogram is significantly different: the degradation of the material is facilitated compared to the other chitosan-based materials: the complete degradation of the material is achieved at 445 °C. The first section of the degradation profile (i.e., below 300 °C) is almost superimposed to GLA-Chit profile, while the final degradation of the material is shifted toward lower temperatures and occurs with a steeper slope. Obviously the presence of the magnetic core leads to the incomplete thermal degradation of the sorbent; the remaining weight fraction of the magnetite in the final product corresponds to the fraction of magnetite in the sorbent (i.e., close to 7.7%). This may explain the low magnetization saturation that was measured by VSM (see above): the fraction of magnetic core is much lower than the amounts incorporated in other magnetic sorbents [33,73]; in addition, the greater the coating layer, the greater the "shielding" effect on magnetic properties [74]. The presence of modified chitosan on the surface of magnetite particles decreases the uniformity due to the quenching of surface moments, which, in turn, reduces the magnetic moment of the composite particles [75].

3.2. Effect of pH on Er(III) sorption

The pH is expected to influence both (a) the speciation of metal ions by formation of hydrolyzed species, or specific complexes in the presence of ligands, and (b) the surface properties of the sorbents by protonation/deprotonation of reactive groups. The presence of carboxylic groups, amine functions, −OH groups and thiol groups, which are characterized by different acid-base properties, leads to proton exchange with the solution: the affinity of these reactive groups is then modulated by the pH of the solution.

These acid-base properties also influence the equilibrium pH. Fig. AM3 (see Additional Material Section) shows the pH variation during metal sorption. Between pH 1 and 3 the equilibrium pH remains almost constant, between pH 3 and pH 4 the equilibrium pH moderately increases (by less than 0.5 pH unit). When the initial pH ranges between 5 and 6 the equibrium pH value may vary by up to 1 or 2 pH units and a kind of "buffering" effect is observed with pH stabilization around 6. Above pH 5 the extent of pH variation decreases, due to this buffering effect. In the sorption of a series of divalent cations on *Saccharomyces cerevisiae* fungal biomass, the buffering capacity was modeled using a four-site acidic model with pK_as values: 3.4 ± 0.4, 5.0 ± 0.2, 6.8 ± 0.4 and 8.9 ± 0.6 [76]. A similar effect is expected with the synthesized sorbent with the coexistence of numerous different reactive groups with different pK_as. Cell is the sorbent that shows the greater pH stability among the five materials. In this case, the main functional

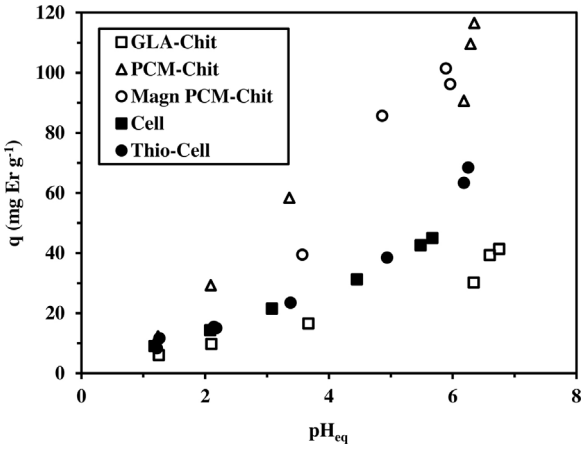

Fig. 7. pH effect on Er(III) sorption using cellulose- and chitosan-based sorbents (C_0: 100 mg Er L^{-1}; T: 300 K; Time: 3 h; Sorbent dosage, SD: 0.2 g L^{-1}).

groups are the R−OH groups, which are the less reactive, in terms of acid-base properties and affinity for metal ions, compared to carboxylic, thiol or amine groups (see below). The significant pH increase is thus alerting on the necessity to strictly control the pH to prevent metal precipitation, at least at high metal concentration. The pH variation observed during metal sorption and the possible occurrence of precipitation phenomena at high metal concentration, especially in the case of sorption isotherms, leaded to set the initial pH value to 5 for further experiments in order to avoid any misinterpretation of metal removal performance.

Fig. 7 shows the impact of equilibrium pH on Er(III) sorption properties. Under selected experimental conditions, the five sorbents show the same sorption capacity (around 10 mg Er g^{-1}) at low pH (i.e., pH close to 1.2): the reactive groups are protonated and then poorly available for the binding of metal cations due to competition effect of protons for binding on reactive groups, and poor ion-exchange properties. When the pH increases the sorption capacity increases almost linearly for GLA-Chit, Cell and Thio-Cell. This is due to the increasing deprotonation of reactive groups such as amine groups or thiol groups in GLA-Chi and Thio-Cell, which progressively increases the affinity of reactive groups for metal ions and decreases the competition effect of protons. The pK_a of thiol compounds immobilized on vermiculite was reported between 8.0 and 8.5 [77]. However, the acid base properties are strongly influenced by the environment of thiol functions [78]. In the case of heavy metal complexation on thiol-containing peptides, Ding et al. [79] reported the shift of the titration curve for the peptides after the binding of metal cations (proving the complexation mechanisms) and they observe that the acid-base characteristics not only depend on the number of thiol groups in the different peptides but also on their global structure. The carboxylic acid moieties in peptides have pK_a values varying, in function of the environment of reactive groups, between 1.85 and 3.49 [80]. Saber-Samandari et al. [44] correlated the effect of the pH on the affinity of nanocomposite membranes, associating carboxymethylated cellulose-graft-poly(acrylic acid)/silica/bentonite for metal ions and dyes to the pH_{zpc} (pH of zero charge) of the sorbents: the pH_{zpc} varied between 4.2 and 4.9 in function of bentonite content.

These results can be correlated to the pH_{ZPC} values of the sorbents reported above: GLA-Chit, Cell and Thio-Cell have very close values of pH_{ZPC} (in the range 6.4-6.6); this means that in the pH range tested for Er(III) sorption these materials are positively charged. The competition effect and charge repulsion contribute to decrease sorption properties, which proceeds through ion-exchange with protons on the sorbents. Obviously, when the pH increases this competition effect decreases and the sorption linearly increases; though sorption properties remain relatively weak compared to chemically modified sorbents. Indeed, for

poly(aminocarboxymethylated) chitosan, as magnetic and non-magnetic composites, the pH_{ZPC} range between 3.7 and 4.5: the carboxylic groups have pK_a values in the range 3–4; as a consequence, the change in surface charge is expected to be more favorable to Er(III) sorption. A significant change (pH-edge) is observed with these sorbents when pH increase with a significant enhancement of sorption performance at pH close to 3–4; this is consistent with observations on Gd(III) and Nd(III) sorption using alfafa biomass [81]: this was correlated to acid-base properties of carboxylic groups and competition effects. The pH-edges curves for Er(III) sorption are shifted toward higher pH values according to the series PCM-Chit < Magn PCM-Chit < Thio-Cell ≈ -Cell < GLA-Chit; this is remarkably consistent with the scale in pH_{ZPC}: 4.12, 4.44, 6.26, 6.21 and 7.05, respectively. This is consistent with the results obtained by Harding and Healy [82] who synthesized a series of amphoteric latex colloids having different values of isoelectric point and different charge-profiles according pH variations. They compared the pH-edges for Cd(II) sorption: the curves were shifted according the series of isoelectric pH values. When the percentage of adsorption is plotted as a function of its pH normalized with respect to the isoelectric point all the curves superimposed on a single profile. They used several declinations of the surface complexation model, with 1:1, 2:1 stoichiometric ratios and/or the binding of $Cd(OH)^+$; they showed that the best match between model and experimental data was obtained when all the interaction modes are involved in Cd(II) binding: Cd(II) 1:1 and 1:2 complexation together with $Cd(OH)^+$ binding. More recently, Eldridge et al. [83] compared the sorption properties of a series of divalent metal cations on different amphoteric polystyrene latices (having amine and carboxyl functional groups). The efficiency of the sorbent is correlated to the equilibrium constant describing metal-carboxyl affinity, which, in turn, is correlated to the isoelectric point and the density of carboxylic groups on the amphoteric polystyrene latices.

In the discussion of pH effect on the sorption of Er(III) onto activated charcoal, Qadeer [84] commented that the distribution coefficient ($K_d = q_{eq}/C_{eq}$) increases with pH due to the decrease in competition effect up to pH 4 and decreases above pH 4 due to the lower affinity of the sorbent for hydrolyzed Er(III) species, which may be under the forms: $Er(OH)^{2+}$, $Er(OH)_2{}^+$, $Er(OH)_3$ and $Er(OH)_4{}^-$. In the case of Eu(III) sorption on chitosan and crab shells, Cadogan et al. [23] proposed the binding of the REE through interactions between different amine groups on adjacent chains of chitosan and simultaneous interactions with C—OH groups (crossed-binding mechanism). In the case of GLA-Chit, a similar mode of action could occur; however, the environment of amine groups is hindered by the chemical bonds with glutaraldehyde: a decrease in sorption is then expected. After the poly (carboxymethylation) of chitosan, the carboxylic groups are supposed to bring additional reactive groups that increase sorption capacities as shown in Fig. 7. Wang et al. [85] discussed the sorption of REEs on alginate/SiO_2 composite. They propose a cation-exchange mechanism involving carboxylic groups and cations, including Ca^{2+}, present as the gelation agent, H^+ and REE^{3+}. The competition between the REE cation and protons in acidic solutions explains the progressive decrease in metal binding when the pH decreases. The binding of the REE(III) cations involves cross-interaction of the metal with carboxylic groups of adjacent polymer chains.

3.3. Uptake kinetics

The sorption processes are kinetically controlled by different mechanisms: the proper reaction rate of sorption, but also resistances to film diffusion and intraparticle diffusion [47]. Indeed, providing a sufficient agitation to prevent concentration gradient and particles settling avoids the resistance to bulk diffusion to contribute to kinetic control. Varying the agitation speed and the size of sorbent particles would help in evaluating the contribution of film diffusion and intraparticle diffusion, respectively. Previous studies on similar materials have shown that the effect of agitation speed and resistance to film diffusion are limited to the very first minutes of contact [86]. The main objective of this work does not consist of an in-deep analysis of diffusion process but to compare the sorption properties of the different biopolymer derivatives. The resistance to film diffusion has been roughly evaluated using the so-called Morris & Weber equation (q(t) is plotted *vs.* the square root of contact time; $q(t) = f(t^{0.5})$ [87]). When the Weber & Morris plot is linear and passes through the origin the mechanism is controlled by the resistance to intraparticle diffusion; when the plot is shifted from the origin the resistance to film diffusion plays a non-negligible effect on kinetic control. On the opposite hand when the plot of q(t) *vs.* $t^{0.5}$ shows several linear sections the mass transfer is generally associated to the co-existence of different diffusion modes corresponding to different porosities of the sorbent. Fig. AM4 (see Additional Material Section) shows the Morris and Weber plots of Er(III) uptake kinetics using the five sorbents at pH 5 (C_0: 100 mg L^{-1}, SD: 0.2 g L^{-1}). The plots are characterized by multi-linear sections: the materials are not homogeneous (in terms of porous characteristics): Cell, Thio-Cell and GLA-Chit show two sections: (a) a first linear section passing through the origin (fast diffusion, within the first 30 min of contact) that corresponds to surface sorption and accumulation within the first external layers of the sorbents, followed by (b) a second section with a very low slope corresponding to equilibrium achievement with slow diffusion to the inner sorption sites. For chitosan derivatives (i.e., PCM-Chit and Magn PCM-Chit) three sections can be identified: (a) 0–30 min with fast sorption (as for other sorbents), (b) 30–150 min with slow diffusion in the core of particles, and (c) above 150 min with progressive achievement of the equilibrium. Resistance to diffusion is thus expected to contribute to the control of uptake kinetics.

Fig. 8 shows the modeling of uptake kinetics using the pseudo-first

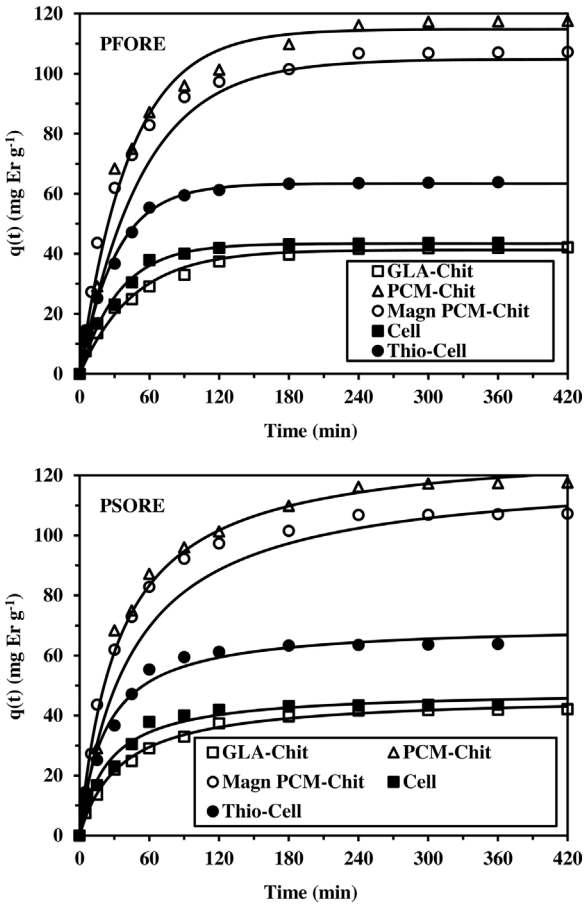

Fig. 8. Uptake kinetics for Er(III) sorption using cellulose- and chitosan-based sorbents – PFORE and PSORE modeling (C_0: 100 mg Er L^{-1}; pH 5; T: 300 K; Sorbent dosage, SD: 0.2 g L^{-1}).

Table 2
Uptake kinetics – Modeling with the PFORE (C_0: 100 mg Er L^{-1}; pH 5; T: 300 K; Sorbent dosage, SD: 0.2 g L^{-1}).

Sorbent	$q_{eq,exp.}$ (mg Er g^{-1})	$q_{eq,calc.}$ (mg Er g^{-1})	$k_1 \times 10^2$ (min^{-1})	R^2
GLA-Chit.	42.15	41.25	2.18	0.991
PCM-Chit.	117.60	114.86	2.34	0.989
Magn PCM-Chit.	107.25	104.84	1.88	0.977
Cellulose	43.65	43.38	2.96	0.987
Thio-Cell.	63.85	63.38	3.19	0.994

Table 3
Uptake kinetics–Modeling with the PSORE (C_0: 100 mg Er L^{-1}; pH 5; T: 300 K; Sorbent dosage, SD: 0.2 g L^{-1}).

Sorbent	$q_{eq,exp.}$ (mg Er g^{-1})	$q_{eq,calc.}$ (mg Er g^{-1})	$k_2 \times 10^4$ (g mg^{-1} min^{-1})	R^2
GLA-Chit.	42.15	46.65	6.11	0.996
PCM-Chit.	117.60	130.53	2.25	0.990
Magn PCM-Chit.	107.25	121.55	1.84	0.976
Cellulose	43.65	48.37	8.49	0.980
Thio-Cell.	63.85	70.47	6.31	0.988

order rate equation (PFORE, Equation AM1, see Additional Material Section) and the pseudo-second order rate equation (PSORE, equation AM2) [45–47]. Tables 2 and 3 summarize the apparent rate coefficients k_1 and k_2, together with the calculated sorption capacity at equilibrium, which can be compared to the experimental value of sorption capacity. These rate parameters should be considered as apparent since these equations were initially developed for modeling homogeneous chemical reactions; the application of these equations to heterogeneous systems means that the apparent rate coefficients integrate the influence of resistances to diffusion. The determination coefficients are of the same order of magnitude for PFORE and PSORE (Tables 2 and 3). In addition, the calculated values for equilibrium sorption capacities ($q_{eq,calc.}$) are significantly overestimated for the PSORE while for the PFORE the calculated values are closer to the experimental sorption capacities ($q_{eq,exp.}$). The PFORE is probably more appropriate for describing the kinetic profiles. The overlapping of the kinetic data with the fitted curve is relatively accurate (Fig. 8) with the exception of Magn PCM-Chit, for which much larger discrepancy is observed, especially before 120 min of contact. For chitosan-based sorbents the apparent rate coefficient (i.e., k_2: 6.1×10^{-4} g mg^{-1} min^{-1}) decreases after poly (aminocarboxymethylation): the rate coefficients are very close for the magnetic and the non-magnetic materials, around 2×10^{-4} g mg^{-1} min^{-1}. For cellulose-based sorbents, the decreasing effect of chemical modification is less marked (Table 3). In the case of the PFORE apparent rate coefficient (i.e., k_1) is slightly higher for cellulose-based materials; however, all the coefficients are weakly varying between 1.8×10^{-2} min^{-1} and 3.2×10^{-2} min^{-1}. Cellulose-based sorbents reach the equilibrium slightly earlier than chitosan-based materials (i.e., 120–150 min against 240–300 min).

3.4. Sorption isotherms and thermodynamics

3.4.1. Sorption isotherms

The sorption isotherms have been established at pH 5 for the five sorbents. Figs. 9 and 10 show the experimental data at different temperatures, in the range 20–50 °C. The solid lines show the fitting of experimental profiles with the Langmuir equation; similar curves are presented for the Freundlich equation in Additional Material Section (Figs. AM5 and AM6 for chitosan-based and cellulose-based sorbents, respectively). Table 4 and AM1 (see Additional Material Section) report the parameters of Langmuir and Freundlich equations for the different

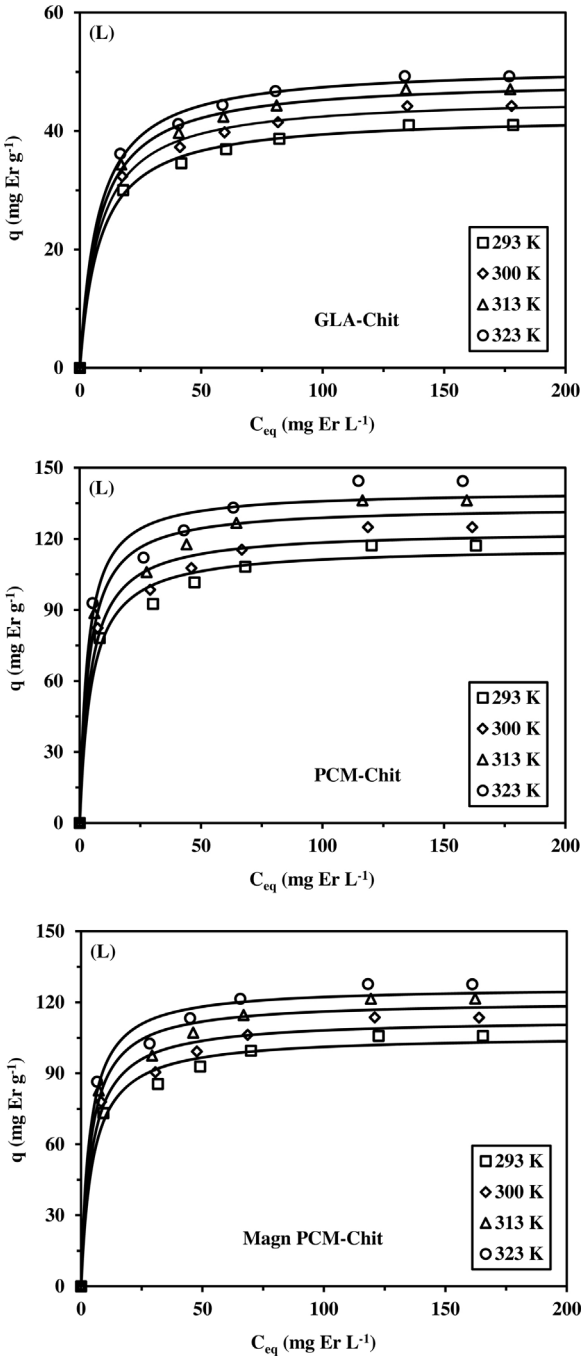

Fig. 9. Er(III) sorption isotherms using chitosan-based sorbents – Langmuir modeling (pH 5; Time: 4 h; Sorbent dosage, SD: 0.2 g L^{-1}).

sorbents, respectively. The determination coefficients (i.e., R^2) are very close for the two models: a little better for Freundlich equation; however, the Langmuir equation that is characterized by an asymptotic trend is more appropriate for describing the binding saturation. Both the maximum sorption capacities (i.e., $q_{m,calc.}$) and the affinity coefficients (*b*) increase with temperature. The sorption process is endothermic. The calculated values (i.e., $q_{m,calc.}$) are very close to the experimental maximum sorption capacities (i.e., $q_{max,exp.}$); differences do not exceed 3%. The sorbents can be ranked according the series:

Cell ≈ GLA-Chit < Thio-Cell < Magn PCM-Chit < PCM-Chit

Yang and Alexandratos [14] correlated the polarizability of donor atom on polymer-supported reagents for the recovery of lanthanides. Lanthanide cations being hard Lewis acids they prefer binding to hard

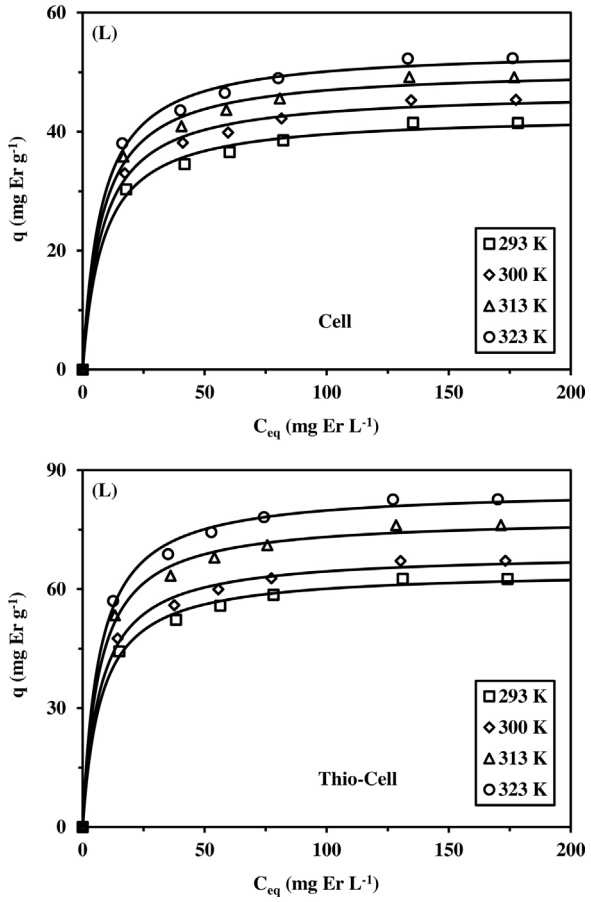

Fig. 10. Er(III) sorption isotherms using cellulose-based sorbents – Langmuir modeling (pH 5; Time: 4 h; Sorbent dosage, SD: 0.2 g L^{-1}).

Table 4
Sorption isotherms – Modeling with the Langmuir equation.

Sorbent	Temp. (°C)	$q_{max,exp.}$ (mg Er g^{-1})	$q_{m,calc.}$ (mg Er g^{-1})	b (L mg^{-1})	R^2
GLA-Chit.	20	41.05	42.64	0.123	0.998
	27	44.25	45.83	0.126	0.998
	40	47.05	48.78	0.128	0.998
	50	49.25	50.98	0.133	0.997
PCM-Chit.	20	117.15	116.66	0.207	0.986
	27	124.95	123.64	0.227	0.984
	40	136.25	133.74	0.268	0.980
	50	144.45	140.31	0.310	0.977
Magn PCM-Chit.	20	105.75	106.05	0.207	0.989
	27	113.55	112.90	0.227	0.986
	40	121.55	120.63	0.256	0.987
	50	127.65	126.59	0.282	0.986
Cellulose	20	41.45	42.83	0.121	0.996
	27	45.35	46.75	0.125	0.996
	40	49.15	50.61	0.129	0.996
	50	52.35	53.93	0.132	0.996
Thio-Cell.	20	62.55	64.64	0.132	0.997
	27	67.15	69.11	0.139	0.997
	40	76.15	78.10	0.148	0.996
	50	82.65	85.20	0.149	0.997

Lewis bases containing oxygen donor atoms preferentially to nitrogen and sulfur donor atoms. The absolute hardness of the ligands decreases following the series OH− (5.6 eV) > NH2- (5.3 eV) > SH− (4.1 eV). Based on this concept deduced from HSAB rules Er(III) sorption is expected to be more efficient on carboxylic groups than on amine groups and even more than on sulfur reactive groups. Although they consider that HSAB is the predominant controlling rule for lanthanide sorption, Yang and Alexandratos also reported the contribution of additional criteria that may influence the affinity order: (a) the basicity or polarizability of the ligand *vs.* the acidity or polarizability of the ion; (b) the effect of the solution on the protonation of the reactive groups; (c) the degree of association of metal ions with counterions; and (d) the extent of hydration of metal ions [14]. These complementary parameters may be used when investigating the selectivity of a sorbent for a series of metal ions in complex solutions; in the case of the comparison of reactive groups for the binding of a given metal ion the first two criteria are the most significant. The effect of pH and protonation/deprotonation of reactive groups was already discussed in the section on pH effect (see above). This may contribute to limit the impact of specific HSAB effects. In addition, the density of reactive groups is much higher for PCM-Chit sorbent (see Table 1 and Section 3.1.1.) than for GLA-Chit: the sorption is then much higher. In the case of Thio-Cell the grafting of additional thiol groups improves the efficiency of sorption but according the HSAB rules the affinity of these reactive groups for Er(III) is weaker compared to amine and carboxylic groups. The differences in maximum sorption capacities between PCM-Chit and Magn PCM-Chit range between 9.7% and 11.6%. The fraction of magnetic core in the composite reaches 7.7% (w/w, as determined by weight loss, in the thermogravimetric studies); this means that the relative amount of modified polymer in the composite magnetic sorbent has decreased in the same order of magnitude than the sorption capacities. The low sorption capacities for GLA-Chit, despite the presence of amine functions is probably due to the specific reaction of amine groups with aldehyde groups of the cross-linking agent: amino groups bound to aldehyde are not available for Er(III) chelation. In the case of Cd(II) binding on cross-linked chitosan, the chemical reaction drastically reduced the reactivity of amine functions [86]. In the study of metal sorption on cellulose, Farrah and Pickering [88] detailed the influence of the pH on sorption efficiency. The presence of two types of acidic functional groups has been identified: one has a pK_a close to 4.4 while the second one has a pK_a close to 7. The acid site is responsible of metal sorption in mild acidic solutions when deprotonation is occurring above pH 4: these reactive groups are mainly associated to the oxidation of CH_2OH groups or to aldehydic end groups of the chain. The density of these reactive groups has been evaluated to 22 meq g^{-1}. The second pK_a (close to 7) corresponds to alcoholic OH groups and can only dissociate at neutral or alkaline pH values, where, in most cases, the metal ions are precipitating (depending on metal concentration); in addition, the density of these groups is relatively low, being quantified to 15 meq g^{-1}. This may explain the capacity of Cell to bind Er(III) but to a weak extent. The grafting of thiol groups increases by 50% the sorption capacity of raw cellulose (i.e., 21–30 mg Er g^{-1}, or 0.13–0.18 mmol Er g^{-1}, depending on the temperature). Table 1 shows that the mass fraction of sulfur element is 1.89% (w/w), which corresponds to a loading of 0.59 mmol −SH per g of sorbent. In the case of the in vitro study of chelation of La(III) with a series of thiols, Yaqoob et al. [89] showed that the affinity of thiol groups increases with their pK_a; in addition they suggest that lanthanum reacts with thiol groups to form $La(RS)_3$ complexes. The increase in sorption capacity due to thiol grafting (i.e., 0.13–0.18 mmol Er g^{-1}) is consistent with the thiol-loading (i.e., 0.59 mmol thiol g^{-1}) for a 1:3 stoichiometric ratio. Thiol groups are very reactive for metal binding especially at low metal concentration [90]. However, the poly(aminocarboxylmethylated) chitosan shows much higher increase in sorption properties (compared to GLA-Chit reference material): maximum sorption capacities are increased by 76–95 mg Er(III) g^{-1} (or 0.46–0.57 mmol Er g^{-1}), and 65–78 mg Er(III) g^{-1} (or 0.39–0.47 mmol Er g^{-1}), respectively; the maximum sorption capacities are increased by 2.8–2.9 for PCM-Chi and 2.6 for Magn PCM-Chit. After poly(aminocarboxymethylation) of the sorbent the nitrogen content increases from 5.33% (w/w) to 6.77% (w/w); which corresponds to 3.80 and 4.83 mmol N g^{-1}, respectively. The

chemical modification brings 1 additional mmol of amine groups per g of sorbent. Based on the suggested structure of the derivative (Fig. 1), this means that the loading of carboxylic groups grafted on the sorbent is close to 1.1 mmol g^{-1}. The increase in maximum sorption capacity for PCM-Chit is mainly due to carboxylic groups although amine groups (strongly hindered) and adjacent −OH groups may contribute to reach the expected coordination number, usually found close to 8–9 [91]. When investigating Cd(II) sorption on Gram + and Gram- bacterial cell walls, Mishra et al. [92] identified the presence of sulfhydryl, carboxyl and phosphoryl reactive groups with very distinct reaction pathway depending on metal concentration: sulfhydryl is only binding Cd(II) at low metal concentration, while when the concentration increases both carboxyl and phosphoryl groups contribute in metal binding. In addition, at the highest metal concentration phosphoryl groups are the predominant reactive groups. With carboxyl and sulfhydryl reactive groups the metal: site reaction stoichiometry is 1:1 indicating a monodentate mechanism, while at low metal concentration and predominance of sulfhydryl groups the multi-dentate binding is characterized by a coordination number higher than one.

The affinity coefficients are of the same order of magnitude for GLA-Chit, Cell and Thio-Cell (around 0.1–0.15 L mg^{-1}); they are halved compared to values of poly(aminocarboxymethylated) sorbents (i.e., 0.2–0.31 L mg^{-1}). Similar trends are observed for the Freundlich modeling of sorption isotherms (Table AM1, see Additional Material Section): the coefficients k_F and n increase with temperature and the rankings for k_F and n follow the same trends as already reported for Langmuir modeling.

3.4.2. Thermodynamic parameters

The thermodynamic characteristics (enthalpy change, ΔH^0, kJ mol^{-1}, Gibbs free energy, ΔG^0, kJ mol^{-1}, and entropy change, ΔS^0, J mol^{-1} K^{-1}) have been determined from sorption isotherms at different temperatures using the Van't Hoff equation by plotting the logarithm of b (affinity coefficient of the Langmuir coefficient) *vs.* the reciprocal of absolute temperature (Fig. AM7, see Additional Material Section):

$$ln(b) = -\frac{\Delta H^0}{RT} + \frac{\Delta S^0}{R} \quad (1)$$

$$\Delta G^0 = \Delta H^0 - T\Delta S^0 \quad (2)$$

Table 5 summarizes these thermodynamic parameters. The positive values of enthalpy change, ΔH^0, confirm that the sorption of Er(III) by the different sorbents is endothermic. For poly(aminocarboxymethylated) derivatives of chitosan the value of the enthalpy change is much higher than the values obtained with not only GLA-Chit but also for cellulose-based materials. This justifies the higher affinity of these sorbents for Er(III). The absolute values $|\Delta G^0|$ are higher than $|T\Delta S^0|$ for GLA-Chit, Cell and Thio-Cell: the sorption of Er(III) is controlled by enthalpic changes rather than entropic changes for these sorbents; a reciprocal trend is observed for poly(aminocarboxymethylated) sorbents. In addition, the Gibbs free energies are higher for chitosan derivatives than for the other sorbents; Er(III) sorption is more spontaneous on these materials. The entropy change is negative for GLA-Chit, Cell and Thio-Cell the system progressively becomes more ordered with the binding of dispersed metal ions on the surface of sorbent particles. A contrary trend is observed for Er(III) sorption with magnetic and non-magnetic PCM-Chit the positive values of entropy change mean that the sorption reaction is entropically driven and this is frequently associated to the release of water, initially bound to metal species, into the solution during metal binding. The chemical modification of GLA-Chit confers to the material a thermodynamic behavior different to its precursor.

3.4.3. Comparison of Er(III) sorption properties with literature data

The sorption of Er(III) is not well documented into the literature. Table 6 summarizes the main sorption characteristics for a series of sorbents. Though some specific resins (for example D113-III carboxylic-type resin [93]) and activated carbon materials [94,95] have shown higher sorption capacities, in the range 250–325 mg Er g^{-1}, poly (aminocarboxymethylated) chitosan demonstrates sorption performances comparable to conventional materials (around 120–140 mg Er g^{-1}). The other sorbents (i.e., GLA-Chit, Cell and Thio-Cell) have much lower sorption capacities, comparable to alumina [96], and extractant-impregnated resins [97,98]. PCM-Chit appears to be the most promising of the synthesized sorbents; depositing the material at the surface of magnetic core particles has a limited effect on uptake kinetics but slightly decreases the sorption capacities.

3.5. Metal desorption and sorbent recycling

The recycling of the sorbent has been investigated using 0.5 M solutions of thiourea, acidified with sulfuric acid at pH 2. The desorption yield was compared over the different cycles, while the sorption capacity was systematically expressed as a percentage of the sorption at

Table 5
Thermodynamic parameters for the sorption of Er(III) using selected sorbents.

Sorbent	Temp. K)	ΔH^0 (kJ mol^{-1})	ΔS^0 (J mol^{-1} K^{-1})	ΔG^0 (kJ mol^{-1})	$T \times \Delta S^0$ (kJ mol^{-1})	R^2
GLA-Chit.	293	1.89	−10.96	5.10	−3.21	0.958
	300			5.18	−3.29	
	313			5.32	−3.43	
	323			5.43	−3.54	
PCM-Chit.	293	10.56	22.90	3.85	6.71	0.997
	300			3.69	6.87	
	313			3.40	7.17	
	323			3.17	7.40	
Magn. PCM-Chit.	293	7.94	14.06	3.82	4.12	0.997
	300			3.72	4.22	
	313			3.54	4.40	
	323			3.40	4.54	
Cellulose	293	2.14	−10.22	5.13	−2.99	0.974
	300			5.20	−3.07	
	313			5.33	−3.20	
	323			5.44	−3.30	
Thio-Cell.	293	3.21	−5.76	4.90	−1.69	0.932
	300			4.94	−1.73	
	313			5.02	−1.80	
	323			5.07	−1.86	

Table 6
Comparison of sorption properties with alternative Er(III) sorbents.

Sorbent	T (°C)	pH	Time (h)	q_m (mg Er g^{-1})	b (L mg^{-1})	Reference
Rice husk-based activated carbon	30	3.5	1	250	0.0048	[77]
Activated charcoal	22	4	1	260	0.0221	[69]
Alumina	45	–	0.25	49	–	[79]
Weakly acidic ion exchange filter	25	6.0	24	142	0.06	[99]
D113-III (resin bearing carboxylic acid groups)	35	6.0	22	325	0.086	[76]
DVB-encapsulated extractant	40	1.8	0.25	54	0.072	[80]
Polysulfone-encapsulated extractant	25	5	1	48	0.080	[81]
GLA-Chit.	27	5	4	46	0.126	This study
PCM-Chit.	27	5	4	124	0.227	This study
Magn PCM-Chit.	27	5	4	113	0.227	This study
Cellulose	27	5	3	47	0.125	This study
Thio-Cell.	27	5	2	69	0.139	This study

Table 7
Metal desorption and sorbent recycling – Relative sorption efficiency (compared to 1st sorption step) and desorption efficiency (relative to corresponding preceding adsorption step).

Cycle	1	2		3		4		5	
Sorbent	Ads. (%)	Ads. (%)	Des. (%)	Ads. (%)	Des. (%)	Ads. (%)	Des. (%)	Ads. (%)	Des. (%)
GLA-Chit.	100	95.15	94.08	93.49	93.02	92.43	93.02	91.48	92.19
PCM-Chit.	100	94.76	93.95	93.05	92.84	91.86	92.84	90.88	91.99
Magn PCM-Chit.	100	95.69	94.73	93.96	93.67	92.31	93.67	90.86	92.00
Cellulose	100	94.44	94.90	93.99	94.33	92.97	93.54	92.18	92.97
Thio-Cell.	100	94.21	94.51	93.22	93.90	92.38	93.22	91.92	92.76

the initial stage. Table 7 reports the sorption and desorption efficiencies obtained for the 5 sorbents at the different cycles. The sorption capacity very slightly decreases at each sorption stage; however, the loss does not exceed 9% at the fifth cycle. The sorbents have a good stability in terms of sorption capacities. The efficiency of desorption slightly decreases from 94% to 92% when comparing the performances at the first and fourth cycles. This means that the variation in metal desorption remains stable and that a small fraction (around 7%) cannot be desorbed from the loaded sorbent. Globally the sorption of the 5 sorbents are comparable and the sorption and desorption efficiencies remain higher than 91% for a minimum of five sorption/desorption cycles.

4. Conclusion

The chemical modifications of cellulose and chitosan (cross-linked with glutaraldehyde) allow increasing Er(III) sorption properties. Thiol groups increase metal sorption on cellulose by 50%, though the best results were obtained with the poly(aminocarboxymethylation) of chitosan: sorption capacities increase from 40–50 mg Er(III) g^{-1} for GLA-Chit to 117–144 mg Er(III) g^{-1} for PCM-Chit. Sorption capacity increases with pH due to the progressive deprotonation of reactive groups (amine functions, thiols groups and carboxylic groups) (depending on the sorbent). The saturation plateau of sorption isotherms is consistent with the Langmuir model, though the Freundlich equation showed very comparable determination coefficients. The sorption capacities also increase with temperature: sorption is endothermic, spontaneous (even increased by the poly(aminocarboxymethylation) of the biopolymer). The main difference between the different sorbents is identified in terms of entropy change: negative for Cell, Thio-Cell and GLA-Chit while positive values are obtained for poly(aminocarboxymethylated) chitosan materials (magnetic and non-magnetic composites showed similar behavior). The kinetic profiles are best fitted by the pseudo-first order rate equation. The incorporation of magnetic core in the composite sorbent does not improves (a) the uptake performance: actually the maximum sorption capacity decreased at the pro-rata of the proportion of inert magnetic core in the material, nor (b) the uptake rate: the equilibrium is reached within the first 4–5 h of contact. All the sorbents can be efficiently desorbed using acidic thiourea solutions (0.5 M) and the sorption and desorption performances decrease at the fifth cycle by less than 9% and 6% for sorption and desorption, respectively. Poly(aminocarboxymethylated) chitosan appears the most promising sorbent for the recovery of Er(III) from weakly acid solutions (pH 5).

Acknowledgements

This work was supported by funding from the International Atomic Energy Agency (IAEA, Vienna, Austria) for TC project number (Oracle Project No.: 1060242) and Fellowship Code No.: C6/EGY/15019). Authors acknowledge Mrs. Momoko Iwai (Hosei University, Japan) for helping for CHN analysis. Special dedication to the memory of Prof. Dr. Ahmed Donia.

Appendix A. Supplementary data

Supplementary data associated with this article can be found, in the online version, at http://dx.doi.org/10.1016/j.colsurfa.2017.05.031.

References

[1] G. Charalampides, K.I. Vatalis, B. Apostoplos, B. Ploutarch-Nikolas, Rare earth elements: industrial applications and economic dependency of Europe, Procedia Econ. Finance 24 (2015) 126–135.
[2] European Commission, Waste Electrical & Electronic Equipment (WEEE), European Commission, Brussels (Belgium), 2016.
[3] K. Binnemans, P.T. Jones, B. Blanpain, T. Van Gerven, Y. Yang, A. Walton, M. Buchert, Recycling of rare earths: a critical review, J. Cleaner Prod. 51 (2013) 1–22.
[4] USEPA, Rare Earth Elements: A Review of Production, Processing, Recycling, and Associated Environmental Issues, Engineering Technical Support Center Land Remediation and Pollution Control Division National Risk Management Research Laboratory Office of Research and Development, U.S.EPA, Cincinnati (OH), USA, 2012 pp. 135.
[5] J. Kulczycka, Z. Kowalski, M. Smol, H. Wirth, Evaluation of the recovery of Rare Earth Elements (REE) from phosphogypsum waste – case study of the WIZOW Chemical Plant (Poland), J. Cleaner Prod. 113 (2016) 345–354.
[6] L.S. Morf, R. Gloor, O. Haag, M. Haupt, S. Skutan, F. Di Lorenzo, D. Boeni, Precious metals and rare earth elements in municipal solid waste – sources and fate in a Swiss incineration plant, Waste Manage. (Oxford) 33 (2013) 634–644.
[7] C. Tunsu, M. Petranikova, C. Ekberg, T. Retegan, A hydrometallurgical process for the recovery of rare earth elements from fluorescent lamp waste fractions, Sep.

Purif. Technol. 161 (2016) 172–186.
[8] K. Habib, K. Parajuly, H. Wenzel, Tracking the flow of resources in electronic waste – the case of end-of-life computer hard disk drives, Environ. Sci. Technol. 49 (2015) 12441–12449.
[9] R. Panda, A. Kumari, M.K. Jha, J. Hait, V. Kumar, J.R. Kumar, J.Y. Lee, Leaching of rare earth metals (REMs) from Korean monazite concentrate, J. Ind. Eng. Chem. 20 (2014) 2035–2042.
[10] F. Xie, T.A. Zhang, D. Dreisinger, F. Doyle, A critical review on solvent extraction of rare earths from aqueous solutions, Miner. Eng. 56 (2014) 10–28.
[11] S. Sinha, Abhilash, P. Meshram, B.D. Pandey, Metallurgical processes for the recovery and recycling of lanthanum from various resources–a review, Hydrometallurgy 160 (2016) 47–59.
[12] S.U. Yesiller, A.E. Eroglu, T. Shahwan, Removal of aqueous rare earth elements (REEs) using nano-iron based materials, J. Ind. Eng. Chem. 19 (2013) 898–907.
[13] E.M. Iannicelli-Zubiani, C. Cristiani, G. Dotelli, P.G. Stampino, R. Pelosato, E. Mesto, E. Schingaro, M. Lacalamita, Use of natural clays as sorbent materials for rare earth ions: materials characterization and set up of the operative parameters, Waste Manage. (Oxford) 46 (2015) 546–556.
[14] Y.J. Yang, S.D. Alexandratos, Affinity of polymer-supported reagents for lanthanides as a function of donor atom polarizability, Ind. Eng. Chem. Res. 48 (2009) 6173–6187.
[15] A. A. H. Abdel-Rahman, I.E.E. El-Aassy, Y.A. Fadia, M.F. Hamza, Studies on the uptake of rare earth elements on polyacrylamidoxime resins from natural concentrate leachate solutions, J. Dispers. Sci. Technol. 31 (2010) 1128–1135.
[16] O.V. Cheremisina, M.A. Ponomareva, V.N. Sagdiev, Thermodynamic characteristics of sorption extraction and chromatographic separation of anionic complexes of erbium and cerium with Trilon B on weakly basic anionite, Russ. J. Phys. Chem. A 90 (2016) 664–670.
[17] B.N. Kumar, S. Radhika, B.R. Reddy, Solid-liquid extraction of heavy rare-earths from phosphoric acid solutions using Tulsion CH-96 and T-PAR resins, Chem. Eng. J. 160 (2010) 138–144.
[18] C.H. Xiong, Y.L. Li, G.T. Wang, L. Fang, S.G. Zhou, C.P. Yao, Q. Chen, X.M. Zheng, D.M. Qi, Y.Q. Fu, Y.F. Zhu, Selective removal of Hg(II) with polyacrylonitrile-2-amino-1, 3, 4-thiadiazole chelating resin: batch and column study, Chem. Eng. J. 259 (2015) 257–265.
[19] Q.X. Zheng, Z.L. Li, X.X. Miao, J.H. Li, Y.F. Huang, H.N. Xia, C.H. Xiong, Preparation and characterization of novel organic chelating resin and its application in recovery of Zn(II) from aqueous solutions, Appl. Organomet. Chem. 31 (2017).
[20] Y. Andrès, A.C. Texier, P. Le Cloirec, Rare earth elements removal by microbial biosorption: a review, Environ. Technol. 24 (2003) 1367–1375.
[21] N. Das, D. Das, Recovery of rare earth metals through biosorption: an overview, J. Rare Earths 31 (2013) 933–943.
[22] A.M. Zoll, J. Schijf, A surface complexation model of YREE sorption on Ulva lactuca in 0. 05–5.0 M NaCl solutions, Geochim. Cosmochim. Acta 97 (2012) 183–199.
[23] E.I. Cadogan, C.-H. Lee, S.R. Popuri, H.-Y. Lin, Efficiencies of chitosan nanoparticles and crab shell particles in europium uptake from aqueous solutions through biosorption: synthesis and characterization, Int. Biodeterior. Biodegrad. 95 (2014) 232–240.
[24] F. Wang, J. Zhao, X. Wei, F. Huo, W. Li, Q. Hu, H. Liu, Adsorption of rare earths (III) by calcium alginate-poly glutamic acid hybrid gels, J. Chem. Technol. Biotechnol. 89 (2014) 969–977.
[25] D. Wu, L. Zhang, L. Wang, B. Zhu, L. Fan, Adsorption of lanthanum by magnetic alginate-chitosan gel beads, J. Chem. Technol. Biotechnol. 86 (2011) 345–352.
[26] F. Wang, J. Zhao, W. Li, H. Zhou, X. Yang, N. Sui, H. Liu, Preparation of several alginate matrix gel beads and their adsorption properties towards rare earths (III), Waste Biomass Valoriz. 4 (2013) 665–674.
[27] E. Guibal, Interactions of metal ions with chitosan-based sorbents: a review, Sep. Purif. Technol. 38 (2004) 43–74.
[28] V.L. Albernaz, G.A. Joanitti, C.A.P. Lopes, L.P. Silva, Cellulose nanocrystals obtained from rice by products and their binding potential to metallic ions, J. Nanomater. (2015), http://dx.doi.org/10.1155/2015/357384.
[29] K. Inoue, K. Ohto, K. Yoshizuka, R. Shinbaru, K. Kina, Adsorption behaviors of some metal-ions on chitosan modified with EDTA-type ligand, Bunseki Kagaku 44 (1995) 283–287.
[30] Y. Takeda, K. Ishida, Thin-layer chromatography of rare earth elements in carboxymethyl cellulose-aqueous sodium chloride systems and the specific separation of yttrium, Bunseki Kagaku 53 (2004) 729–734.
[31] J. Roosen, K. Binnemans, Adsorption and chromatographic separation of rare earths with EDTA- and DTPA-functionalized chitosan biopolymers, J. Mater. Chem. A 2 (2014) 1530–1540.
[32] J. Roosen, J. Spooren, K. Binnemans, Adsorption performance of functionalized chitosan-silica hybrid materials toward rare earths, J. Mater. Chem. A 2 (2014) 19415–19426.
[33] A.A. Galhoum, M.G. Mahfouz, S.T. Abdel-Rehem, N.A. Gomaa, A.A. Atia, T. Vincent, E. Guibal, Diethylenetriamine-functionalized chitosan magnetic nano-based particles for the sorption of rare earth metal ions Nd(III), Dy(III) and Yb(III), Cellulose 22 (2015) 2589–2605.
[34] S. Hokkanen, A. Bhatnagar, M. Sillanpaa, A review on modification methods to cellulose-based adsorbents to improve adsorption capacity, Water Res. 91 (2016) 156–173.
[35] Y. Zhu, Y. Zheng, A. Wang, A simple approach to fabricate granular adsorbent for adsorption of rare elements, Int. J. Biol. Macromol. 72 (2015) 410–420.
[36] T.L. Ho, Hard and soft acids bases (HSAB) principle and organic-chemistry, Chem. Rev. 75 (1975) 1–20.
[37] R.G. Pearson, Acids and bases, Science 151 (1966) 172–177.
[38] J. Chung, J. Chun, J. Lee, S.H. Lee, Y.J. Lee, S.W. Hong, Sorption of Pb(II) and Cu(II) onto multi-amine grafted mesoporous silica embedded with nano-magnetite: effects of steric factors, J. Hazard. Mater. 239 (2012) 183–191.
[39] K. Li, Q. Gao, G. Yadavalli, X. Shen, H. Lei, B. Han, K. Xia, C. Zhou, Selective adsorption of Gd^{3+} on a magnetically retrievable imprinted chitosan/carbon nanotube composite with high capacity, ACS Appl. Mater. Interfaces 7 (2015) 21047–21055.
[40] M.C. Gennaro, C. Baiocchi, E. Campi, E. Mentasti, R. Aruga, Preparation and characterization of iminodiacetic acid cellulose filters for concentration of trace-metal cations, Anal. Chim. Acta 151 (1983) 339–347.
[41] T.L. Vigo, C.M. Welch, Chlorination and phosphorylation of cotton cellulose by reaction with phosphoryl chloride in N,N-dimethylformamide, Carbohydr. Res. 32 (1974) 331–338.
[42] T. Tashiro, Y. Shimura, Removal of mercuric ions by systems based on cellulose derivatives, J. Appl. Polym. Sci. 27 (1982) 747–756.
[43] A.A. Galhoum, A.A. Atia, M.G. Mahfouz, S.T. Abdel-Rehem, N.A. Gomaa, T. Vincent, E. Guibal, Dy(III) recovery from dilute solutions using magnetic-chitosan nano-based particles grafted with amino acids, J. Mater. Sci. 50 (2015) 2832–2848.
[44] S. Saber-Samandari, S. Saber-Samandari, S. Heydaripour, M. Abdouss, Novel carboxymethyl cellulose based nanocomposite membrane: synthesis, characterization and application in water treatment, J. Environ. Manage. 166 (2016) 457–465.
[45] Y.S. Ho, G. McKay, Pseudo-second order model for sorption processes, Proc. Biochem. 34 (1999) 451–465.
[46] S. Lagergren, About the theory of so-called adsorption of soluble substances, Kungliga Svenska Vetenskapsakademiens 24 (1898) 1–39.
[47] C. Tien, Adsorption Calculations and Modeling, Butterworth-Heinemann, Newton, MA, 1994.
[48] K.Y. Foo, B.H. Hameed, Insights into the modeling of adsorption isotherm systems, Chem. Eng. J. 156 (2010) 2–10.
[49] H.M.F. Freundlich, Uber die adsorption in lasungen, Z. Phys. Chem. 57 (1906) 385–470.
[50] I. Langmuir, The adsorption of gases on plane surfaces of glass, mica and platinum, J. Amer. Chem. Soc. 40 (1918) 1361–1402.
[51] M. Ibrahim, O. Osman, A.A. Mahmoud, Spectroscopic analyses of cellulose and chitosan: FTIR and modeling approach, J. Comput. Theor. Nanosci. 8 (2011) 117–123.
[52] D. Ciolacu, F. Ciolacu, V.I. Popa, Amorphous cellulose – structure and characterization, Cellul. Chem. Technol. 45 (2011) 13–21.
[53] J. Coates, Interpretation of infrared spectra, a practical approach, in: R.A. Meyers (Ed.), Encyclopedia of Analytical Chemistry, John Wiley & Sons Ltd, Chichester, U.K, 2000, pp. 10815–10837.
[54] E.C. Silva Filho, L.C.B. Lima, F.C. Silva, K.S. Sousa, M.G. Fonseca, S.A.A. Santana, Immobilization of ethylene sulfide in aminated cellulose for removal of the divalent cations, Carbohydr. Polym. 92 (2013) 1203–1210.
[55] A.A. Tolba, S.I. Mohamady, S.S. Hussin, T. Akashi, Y. Sakai, A.A. Galhoum, E. Guibal, Synthesis and characterization of poly(carboxymethyl)-cellulose for enhanced La(III) sorption, Carbohydr. Polym. 157 (2017) 1809–1820.
[56] A.M. Donia, A.M. Yousif, A.A. Atia, H.M. Abd El-Latif, Preparation and characterization of modified cellulose adsorbents with high surface area and high adsorption affinity for Hg(II), J. Dispers. Sci. Technol. 35 (2014) 380–389.
[57] J. Jin, X. Huang, L. Zhou, J. Peng, Y. Wang, In situ preparation of magnetic chitosan resins functionalized with triethylene-tetramine for the adsorption of uranyl(II) ions, J. Radioanal. Nucl. Chem. 303 (2015) 797–806.
[58] M.L. Duarte, M.C. Ferreira, M.R. Marvao, J. Rocha, An optimised method to determine the degree of acetylation of chitin and chitosan by FTIR spectroscopy, Int. J. Biol. Macromol. 31 (2002) 1–8.
[59] K. Van de Velde, P. Kiekens, Structure analysis and degree of substitution of chitin, chitosan and dibutyrylchitin by FT-IR spectroscopy and solid state C-13 NMR, Carbohydr. Polym. 58 (2004) 409–416.
[60] R.S. Vieira, M.M. Beppu, Interaction of natural and crosslinked chitosan membranes with Hg(II) ions, Colloids Surf. A 279 (2006) 196–207.
[61] E. Igberase, P. Osifo, A. Ofomaja, Chromium (VI) ion adsorption by grafted cross-linked chitosan beads in aqueous solution – a mathematical and statistical modeling study, Environ. Technol. (2017) 1–11.
[62] L.S. Silva, L.C.B. Lima, F.C. Silva, J.M.E. Matos, M.R.M.C. Santos, L.S. Santos Junior, K.S. Sousa, E.C. da Silva Filho, Dye anionic sorption in aqueous solution onto a cellulose surface chemically modified with aminoethanethiol, Chem. Eng. J. 218 (2013) 89–98.
[63] I.A. Udoetok, R.M. Dimmick, L.D. Wilson, J.V. Headley, Adsorption properties of cross-linked cellulose-epichlorohydrin polymers in aqueous solution, Carbohydr. Polym. 136 (2016) 329–340.
[64] A. Isogai, M. Usuda, T. Kato, T. Uryu, R.H. Atalla, Solid-state CP/MAS carbon-13 NMR study of cellulose polymorphs, Macromolecules 22 (1989) 3168–3172.
[65] S. Naduparambath, E. Purushothaman, Sago seed shell: determination of the composition and isolation of microcrystalline cellulose (MCC), Cellulose 23 (2016) 1803–1812.
[66] A.K. Veeramachineni, T. Sathasivam, S. Muniyandy, P. Janarthanan, S.J. Langford, L.Y. Yan, Optimizing extraction of cellulose and synthesizing pharmaceutical grade carboxymethyl Sago cellulose from Malaysian Sago pulp, Appl. Sci. – Basel 6 (2016).
[67] F.C. Vasconcellos, G.A.S. Goulart, M.M. Beppu, Production and characterization of chitosan microparticles containing papain for controlled release applications, Powder Technol. 205 (2011) 65–70.
[68] F.P. Zhao, E. Repo, M. Sillanpaa, Y. Meng, D.L. Yin, W.Z. Tang, Green synthesis of magnetic EDTA- and/or DTPA-cross-linked chitosan adsorbents for highly efficient removal of metals, Ind. Eng. Chem. Res. 54 (2015) 1271–1281.

[69] M.G. Mahfouz, A.A. Galhoum, N.A. Gomaa, S.S. Abdel-Rehem, A.A. Atia, T. Vincent, E. Guibal, Uranium extraction using magnetic nano-based particles of diethylenetriamine-functionalized chitosan: equilibrium and kinetic studies, Chem. Eng. J. 262 (2015) 198–209.
[70] J. Zhang, S. Zhang, Y. Wang, J. Zeng, Composite magnetic microspheres: preparation and characterization, J. Magn. Magn. Mater. 309 (2007) 197–201.
[71] G.-y. Li, Z.-d. Zhou, Y.-j. Li, K.-l. Huang, M. Zhong, Surface functionalization of chitosan-coated magnetic nanoparticles for covalent immobilization of yeast alcohol dehydrogenase from Saccharomyces cerevisiae, J. Magn. Magn. Mater. 322 (2010) 3862–3868.
[72] R.M. Patil, P.B. Shete, N.D. Thorat, S.V. Otari, K.C. Barick, A. Prasad, R.S. Ningthoujam, B.M. Tiwale, S.H. Pawar, Superparamagnetic iron oxide/chitosan core/shells for hyperthermia application: improved colloidal stability and biocompatibility, J. Magn. Magn. Mater. 355 (2014) 22–30.
[73] A.A. Galhoum, M.G. Mafhouz, S.T. Abdel-Rehem, N.A. Gomaa, A.A. Atia, T. Vincent, E. Guibal, Cysteine-functionalized chitosan magnetic nano-based particles for the recovery of light and heavy rare earth metals: uptake kinetics and sorption isotherms, Nanomaterials 5 (2015) 154–179.
[74] H. Yan, H. Li, H. Yang, A. Li, R. Cheng, Removal of various cationic dyes from aqueous solutions using a kind of fully biodegradable magnetic composite microsphere, Chem. Eng. J. 223 (2013) 402–411.
[75] L.-y. Zhang, X.-j. Zhu, H.-w. Sun, G.-r. Chi, J.-x. Xu, Y.-l. Sun, Control synthesis of magnetic Fe3O4–chitosan nanoparticles under UV irradiation in aqueous system, Curr. Appl Phys. 10 (2010) 828–833.
[76] A. Naeem, J.R. Woertz, J.B. Fein, Experimental measurement of proton, Cd, Pb, Sr, and Zn adsorption onto the fungal species Saccharomyces cerevisiae, Environ. Sci. Technol. 40 (2006) 5724–5729.
[77] F.H. do Nascimento, D.M. de Souza Costa, J.C. Masini, Evaluation of thiol-modified vermiculite for removal of Hg(II) from aqueous solutions, Appl. Clay Sci. 124 (2016) 227–235.
[78] A. Mirzahosseini, B. Noszál, The species- and site-specific acid–base properties of biological thiols and their homodisulfides, J. Pharm. Biomed. Anal. 95 (2014) 184–192.
[79] X. Ding, Y. Hua, Y. Chen, C. Zhang, X. Kong, Heavy metal complexation of thiol-containing peptides from soy glycinin hydrolysates, Int. J. Mol. Sci. 16 (2015) 8040–8058.
[80] R.R. Khoury, G.J. Sutton, D.B. Hibbert, D. Ebrahimi, Measurement and modeling of acid dissociation constants of tri-peptides containing Glu, Gly, and His using potentiometry and generalized multiplicative analysis of variance, Dalton Trans. 42 (2013) 2940–2947.
[81] J.G. Parsons, J.R. Peralta-Videa, K.J. Tiemann, G.B. Saupe, J.L. Gardea-Torresdey, Use of chemical modification and spectroscopic techniques to determine the binding and coordination of gadolinium(III) and neodymium(III) ions by alfalfa biomass, Talanta 67 (2005) 34–45.
[82] I.H. Harding, T.W. Healy, Adsorption of aqueous candmium(II) on amphoteric latex colloids. 2. isoelectric point effects, J. Colloid Interface Sci. 107 (1985) 371–381.
[83] D.S. Eldridge, R.J. Crawford, I.H. Harding, The role of metal ion-ligand interactions during divalent metal ion adsorption, J. Colloid Interface Sci. 454 (2015) 20–26.
[84] R. Qadeer, Adsorption of erbium ions on activated charcoal from aqueous solutions, Colloids Surf. A 254 (2005) 17–21.
[85] F. Wang, J. Zhao, F. Pan, H. Zhou, X. Yang, W. Li, H. Liu, Adsorption properties toward trivalent rare earths by alginate beads doping with silica, Ind. Eng. Chem. Res. 52 (2013) 3453–3461.
[86] M.S.D. Erosa, T.I.S. Medina, R.N. Mendoza, M.A. Rodriguez, E. Guibal, Cadmium sorption on chitosan sorbents: kinetic and equilibrium studies, Hydrometallurgy 61 (2001) 157–167.
[87] W.J. Weber, J.C. Morris, Kinetics of adsorption on carbon from solutions, J. Sanit. Eng. Div. ASCE 89 (1963) 31–60.
[88] H. Farrah, W.F. Pickering, Effect of pH and ligands on sorption of heavy-metal ions by cellulose, Aust. J. Chem. 31 (1978) 1501–1509.
[89] Muhammad Yaqoob, Muhammad Farid Khan, Muhammad Tausif Chaudhry, I.A. Shaikh, Chelation of lanthanum (La^{3+}) by various thiols–an in vitro study, Int. J. Pharmacol. Clin. Sci. 3 (2014) 34–38.
[90] Q. Yu, J. Szymanowski, S.C.B. Myneni, J.B. Fein, Characterization of sulfhydryl sites within bacterial cell envelopes using selective site-blocking and potentiometric titrations, Chem. Geol. 373 (2014) 50–58.
[91] Q. Zhou, H. Yang, C.J. Yan, W.J. Luo, X.J. Li, J.J. Zhao, Synthesis of carboxylic acid functionalized diatomite with a micro-villous surface via UV-induced graft polymerization and its adsorption properties for Lanthanum(III) ions, Colloids Surf. A 501 (2016) 9–16.
[92] B. Mishra, M. Boyanov, B.A. Bunker, S.D. Kelly, K.M. Kemner, J.B. Fein, High- and low-affinity binding sites for Cd on the bacterial cell walls of Bacillus subtilis and Shewanella oneidensis, Geochim. Cosmochim. Acta 74 (2010) 4219–4233.
[93] C. Xiong, Y. Meng, C. Yao, C. Shen, Adsorption of erbium(III) on D113-III resin from aqueous solutions: batch and column studies, J. Rare Earths 27 (2009) 923–931.
[94] N.S. Awwad, H.M.H. Gad, M.I. Ahmad, H.F. Aly, Sorption of lanthanum and erbium from aqueous solution by activated carbon prepared from rice husk, Colloids Surf. B 81 (2010) 593–599.
[95] R. Qadeer, Kinetic study of erbium ion adsorption on activated charcoal from aqueous solutions, Adsorption 11 (2005) 51–55.
[96] M. Saleem, M. Afzal, F. Mahmood, A. Ali, Surface characterization and thermodynamics of adsorption of Pr, Nd and Er on alumina for aqueous solution, Adsorpt. Sci. Technol. 9 (1992) 17–29.
[97] E. Karnio, Y. Fujiwara, M. Mats Urnoto, F. Valenzuela, K. Kondo, Investigation on extraction rate of lanthanides with extractant-impregnated microcapsule, Chem. Eng. J. 139 (2008) 93–105.
[98] Y. Wang, Y. Wang, Y. Jing, J. Chen, Y. Liu, Microcapsules containing ionic liquid [A336][P507] for La^{3+}/Sm^{3+}/Er^{3+} recovery from dilute aqueous solution, J. Rare Earths 34 (2016) 1260–1268.
[99] C. Xiong, C. Yao, Preparation and application of acrylic acid grafted polytetrafluoroethylene fiber as a weak acid cation exchanger for adsorption of Er(III), J. Hazard. Mater. 170 (2009) 1125–1132.